

Foams out of stable equilibrium: cell elongation and side swapping

F. ELIAS^{†‡}, C. FLAMENT^{†‡}, J. A. GLAZIER[§], F. GRANER[¶] ¶
and Y. JIANG^{§††}

[†] Laboratoire des Milieux Désordonnés et Hétérogènes (case 78), Université Paris 6 and Unité Mixte de Recherche associée au CNRS 7603, 4 place Jussieu, 75252 Paris Cedex 05, France

[‡] Université Paris 7, Denis Diderot, Unité de Formation et de Recherche de Physique (case 70.08), 2 place Jussieu, 75051 Paris Cedex 05, France

[§] Department of Physics, 316 Nieuwland, University of Notre-Dame, Notre-Dame, Indiana 46556-5670, USA

[¶] Unité Mixte de Recherche associée au CNRS 5588 et Université Grenoble I—Joseph Fourier, Laboratoire de Spectrométrie Physique, BP 87, 38402 Saint Martin d'Hères, France

[Received 5 October 1998 and accepted 8 December 1998]

ABSTRACT

The evolution of a liquid foam usually mixes quasi-equilibrium topological and geometrical features in an intricate way. We take advantage of special properties of ferrofluid froths and of constrained area evolution simulations, to distinguish the effects of side swapping (T1 processes) from other rearrangements in the froth. Cell elongation characterizes the froth and its deviation from mechanical equilibrium as robustly as the usually measured total wall length, that is surface energy.

§1. INTRODUCTION

Three-dimensional (3D) liquid foams, that is a small volume fraction of liquid forming a continuous network and separating fluid-filled cells (Kraynik 1988), have an intriguing characteristic. Two *a priori* unrelated quantities are correlated (Glazier 1993): firstly the Gaussian curvature of a cell's walls, related to its number of neighbours, that is its topology, and secondly the mean curvature of its walls, related to its internal pressure via Laplace's law, which governs the dynamical evolution of its volume. These quantities are equivalent only for a sphere; the correlation means that cells in a soap froth are nearly round, which is not true in arbitrary cellular patterns. How can we understand this correlation?

For simplicity, we shall consider only *a liquid foam with fixed cell number and volumes* (in a coarsening foam, we would consider only time scales much shorter than the characteristic time for cell volume variation). Such foam relaxes in a finite time towards an equilibrated pattern, corresponding to a local minimum of surface

¶ Author for correspondence: Email: graner@ujf-grenoble.fr.

†† Present address: T-CNLS, MS B258, Los Alamos National Laboratory, New Mexico 87545, USA.

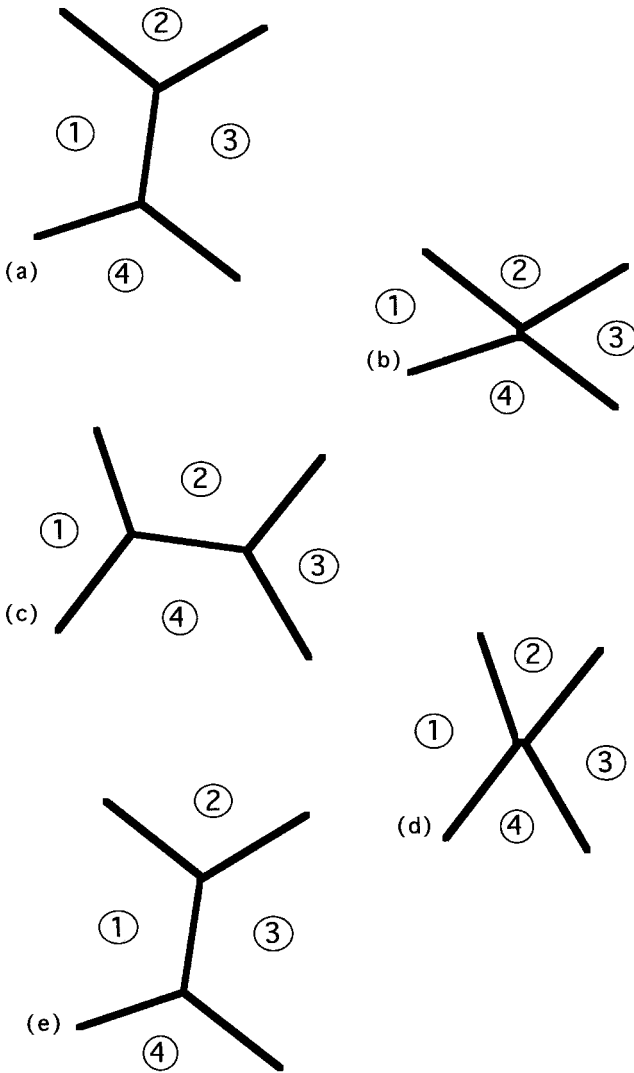


Figure 1. Side swapping (T1 processes). (a) The initial configuration has two threefold vertices. (b) When the side length decreases to zero, an unstable fourfold vertex appears and eventually decays into a new local energy minimum. (c) Cells 1 and 3 lose one side. The reverse T1 (c)–(e) occurs via a different unstable fourfold vertex (d).

energy. It is metastable under an infinitesimal strain; only a change in cell volumes or a finite strain would force a T1 process (side swapping (figure 1)) and a relaxation towards another metastable pattern. In the multistability lies the rich complexity of foam behaviour.

Amongst all possible metastable patterns, an unsheared foam selects only patterns with nearly round cells, which minimize their wall surface for fixed gas content. However, a foam is deterministic; no thermal fluctuation induces any ergodic exploration of different patterns, and three questions arise.

- (1) How is surface energy minimized?

- (2) Does this minimization ultimately reach the lowest energy level, for fixed cell number and volumes, that is the global energy minimum (possibly degenerate) corresponding to at least one truly stable pattern?
- (3) If not, what is the difference between the energy of a selected pattern and the true global energy minimum?

The present study uses two-dimensional (2D) liquid froths, where the selection problem is the same as in three dimensions, but much easier to study in experiment, simulation and theory (Glazier 1989). In two dimensions, it is tedious but easy to determine whether a pattern is in (metastable) equilibrium. For given cell areas, check whether all vertices are threefold and walls meet at 120° ; also check that pressure difference across walls are transitive; that is, on any closed path, the curvatures of the walls we cross sum to zero, according to the Young–Laplace law. However, if we look at a picture of a froth, can we tell at once whether it is in a global energy minimum? Here, the answer is not easy. Conventional measurements of a soap froth (boundary lengths, topological and area distributions, their correlations, and the second moments of these distributions) do not help. While cell elongation has often been used to describe qualitatively the deviations from regular patterns, nobody has precisely addressed the relation between cell elongation and froth evolution.

In this paper, we provide an easy quantitative test, to answer questions (1)–(3) for any given picture of a 2D cellular pattern. We take advantage of special properties of ferrofluid froths and of constrained area evolution simulations to study the effects of individual T1s, both natural and artificial. We define and then measure the elongation of cells; we claim that it marks the deviation from the global energy minimum.

§2. METHODS

In this section, we describe experiments with magnetic fluids and simulations with the Potts model. We chose foams with conserved areas to distinguish coarsening from T1 events. These model systems enabled us to observe single T1s in detail and even to force them.

2.1. Experiment

2D ferrofluid froths have been described in detail elsewhere (Elias *et al.* 1997). Immiscible oil and water are placed between two horizontal Plexiglas plates. Magnetic colloidal particles are stably incorporated into the aqueous phase, so that when an external magnetic field H is applied perpendicular to the plates, magnetic dipole–dipole repulsion tends to stretch the aqueous phase. This stretching competes with the surface tension of the oil–water interface induced by van der Waals attraction, resulting in long-lasting 2D foams (figure 2(2)). These foams consist of domains of oil separated by aqueous walls. After a period of equilibration, the pattern reaches a static equilibrium in which cells neither grow nor shrink at the fixed control parameter H . The equilibrium thickness of the ferrofluid walls decreases with increasing H (Elias *et al.* 1998b). The volume of ferrofluid is fixed; the total equilibrium length of the boundaries, and consequently the equilibrium number of cells in the foam, increase with increasing H .

The foam nucleates with H of the order of 10 kA m^{-1} – 120 G. If H later decreases, some cells must disappear and wall breakage allows the foam to coarsen

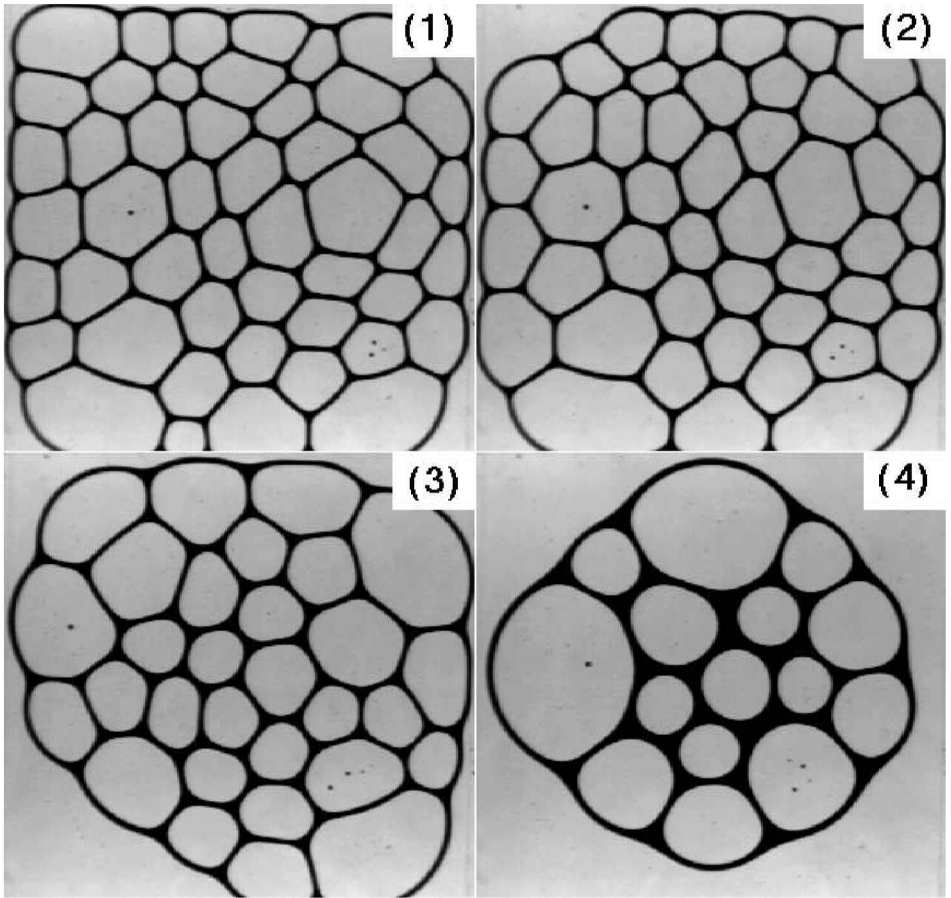


Figure 2. Images of a $10\text{ cm} \times 10\text{ cm}$ froth (ferrofluid fraction $\phi = 0.13$). The pattern evolution is dominated by the external magnetic field H perpendicular to the plane of the image. The foam was nucleated at $H = 11.19\text{ kA m}^{-1}$. Decreasing the field decreases the total wall length of the foam, analogous to increasing time in soap froths. (1) $H = 11.19\text{ kA m}^{-1}$; (2) $H = 9.15\text{ kA m}^{-1}$; (3) $H = 7.50\text{ kA m}^{-1}$; (4) $H = 6.27\text{ kA m}^{-1}$. See other examples in the paper by Elias *et al.* (1997).

(figure 2(3)). In the limit of zero external field, the pattern turns into a single ferrofluid drop surrounded by oil.

On the other hand, in the absence of cell nucleation, if H increases, the pattern disequilibrates (Elias *et al.* 1998a)†. Since the oil wets the Plexiglas better than the water, a thin film of oil actually connects the cells and makes a (slow) time evolution possible. Cells which have fewer than six sides grow, whereas cells which have more than six sides shrink, and six-sided cells do not evolve. This growth law resembles von Neumann's law for two dimensions coarsening soap froths, but with reversed dependence on topology, and without cell disappearance. Before they become too small, the seven-sided cells lose one side through a T1 and stop shrinking. The five-sided cells grow and their neighbours stretch, as shown in figure 2(1).

† A rapid increase in H yields a dynamical elongation of cell walls, resulting in a transient undulation instability.

Ferrofluid froths are ideal archetypes to study T1s for the following reasons.

First, cell areas remain constant at fixed H , as discussed above.

Second, ferrofluid foams are easy to observe. Walls are visible with high contrast. Cells are large, typically 1 cm. Vertex movement is slow, so that T1s can be conveniently observed on a scale of few seconds, but allow observation of many individual events within minutes. We turn to simulations when we need statistics on many cells.

Third, in ferrofluid froths, the external magnetic field plays the role that time plays in soap froth. This control parameter can be easily tuned, ramped, stabilized or reversed; the froth evolves accordingly (Elias *et al.* 1997). Thus, instead of simply watching the time evolution of the froth, we can control it.

Fourth, instead of simply waiting for spontaneous T1s, we can artificially force them (Elias *et al.* 1997, 1998b). A piece of magnetic metal, say a needle, placed over the experimental sample, channels the field lines and locally increases the external field. Magnetic fluid drains and accumulates in this higher-field region. Placing a needle near a vertex displaces the vertex towards the needle. Movements of up to a cell size, that is a centimetre, are possible. Removing the needle relaxes the vertex position and sometimes causes a T1 (see §4.2).

2.2. Simulations

Simulations of T1s in froth under shear using the extended large- Q Potts model have been presented elsewhere (Jiang *et al.* 1998). The great advantage of the large- Q Potts model is its simplicity (Glazier *et al.* 1990). The model is ‘realistic’ in that the position and diffusion of the boundaries determine the dynamics, as they do in real foams and concentrated emulsions. The large- Q Potts model partitions space into domains of lattice sites. Each domain (cell) corresponds to a ‘spin’ value σ_i while the domain boundaries (cell walls) are links between different spins. Thus unlike the situation in magnetic materials, each spin value merely acts as a label for a particular cell. The surface energy resides on the boundaries only. Cells have geometric properties as well as surface properties. Simulations using the large- Q Potts model on low-anisotropy lattices reproduce accurately the time evolution of 2D soap foams (Holm *et al.* 1991).

Since the present study focuses on shear-driven topological rearrangements, we prohibit foam coarsening by applying an area constraint on individual cells, that is deviation from the target areas contributes to a bulk energy and is unfavourable. This constraint also eliminates cell disappearance (T2 processes). The total energy of the froth thus consists of a surface energy and an elastic bulk energy. We extended the Potts Hamiltonian H_P to apply shear strain:

$$H_P = \sum_{\text{neighbouring sites } i,j} J_{ij}(1 - \delta_{\sigma_i,\sigma_j}) + \sum_{\text{cell } n} (a_n - A_n)^2 + \sum_{\text{site } i} \gamma(y_i, t) \Delta x_i,$$

where J_{ij} and σ_i are the coupling strength and spin respectively; a_n and A_n are the area of the n th cell and its corresponding area under zero applied strain respectively. The last term corresponds to applying shear, with γ the strain field and Δx_i the displacement of the spin in the direction of the strain.

The evolution of the froth follows Monte Carlo dynamics. At each Monte Carlo step (MCS), the following procedure is performed N times, where N is the total number of boundary lattice sites. A site is randomly chosen from the domain boundary sites (cell walls), and the spin at the site is reassigned to the spin value of one of

its neighbours; the probability P of accepting the reassignment depends on the energy change ΔH_P caused by the spin flip:

$$P = \begin{cases} 1 & (\Delta H_P < 0), \\ \exp\left(-\frac{\Delta H_P}{T}\right) & (\Delta H_P \geq 0). \end{cases}$$

The shear term biases P in the direction of increasing ($\gamma < 0$) or decreasing ($\gamma > 0$) x_i . Since in the Potts model the speed of cell wall migration is proportional to P , this term effectively enforces a velocity v , that is applies a strain rate to the foam. The strain is proportional to a time integral of v , and γ is related to the amplitude of strain.

We can freely adjust the range of the strain to apply either boundary strain (applied to the boundary of the froth only) or bulk strain (strain amplitude varying linearly through the froth). In this model, we keep a record of the number of sides for each cell. Since cell disappearance is prohibited, a change in cell topology indicates a T1.

2.3. Comparison between experiments and simulations

In the Potts model simulations, when a single cell is stretched and released, its largest diameter decreases as $\exp(-t/\tau)$ as it rounds. We define τ as the relaxation time scale, which is of the order of 10 MCSs with the simulation parameters that we used (Jiang *et al.* 1998). In experiments, the typical time scale of the order of 1 s is due to surface viscous drag and geometric confinement by other cells. In practical applications to coarsening foams, the time scale τ of foam deformation and relaxation is often much faster than diffusion of the filling fluid; so neglecting coarsening is reasonable. For instance, in experiments, the cell area is not actually conserved, but its variation rate about $10^{-2} \text{ mm}^2 \text{ s}^{-1}$ is so slow that it is negligible.

In simulations, the area constraint is almost always satisfied, that is the deviation of each cell's area from its target value contributes a negligible energy, less than one thousandth of the surface energy. In comparison with simulations or classical experiments with soap froths, our ferrofluid foams have an additional energy, difficult to quantify, due to magnetic dipolar repulsions between ferrofluid walls; since it apparently did not affect the results presented below, we did not take it into account in the simulations, although we could. This choice is validated *a posteriori* by the agreement between experiment and simulation.

Note that both the experimental and the numerical foams have a rather mono-dispersed distribution of sizes and side numbers, and remain monodispersed owing to the cell area conservation.

§3. ANALYSIS OF CELL ELONGATION

3.1. Definitions

Elongation, the qualitative notion that a cell is not circular, can be quantified in different ways, with varying advantages and disadvantages (figure 3).

The classical definition is the ratio of the largest cell diameter to the smallest cell diameter, because it considers only two diameters, it is insensitive to details of the shape and oversensitive to noise.

The eccentricity of the cell, defined as the ratio of the largest principal moment of inertia to the smallest principal moments of inertia, is robust. However, it does not

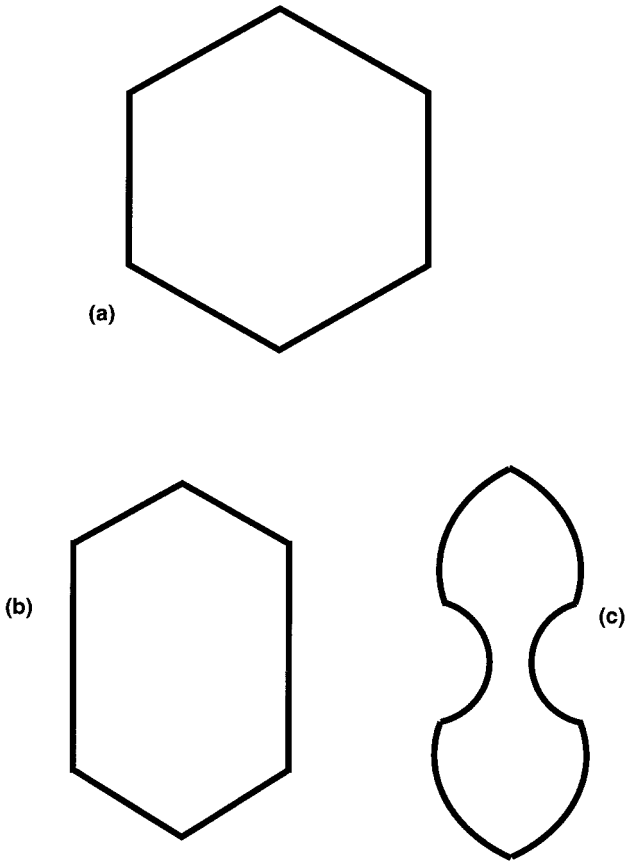


Figure 3. Examples of hexagons with different elongations. (a) Regular hexagon: the ratio of the largest diameter to the smallest diameter is two; the inertia matrix is isotropic and thus has zero eccentricity; the variance of the side length is zero; $PA^{1/2} = (PA^{1/2})_6 = 3.72$. (b) Stretched hexagon: these four quantities have strictly increased. (c) Curved walls: same ratio of the largest diameter to the smallest diameter as in (b), larger eccentricity and $PA^{1/2}$, zero side length variance.

suit our purpose because it has the same value for, say, a regular hexagon with straight or concave walls (see figure 3). It is thus insensitive to the fact that the concavity increases the wall length and decreases the cell area. Moreover, trials on experimental and simulated foams showed that the eccentricity does not reflect the expert's intuition, in the sense that the measured eccentricity sometimes increases while intuitively we see that the cell's irregularity decreases.

The variance σ of the side length distribution, hereafter referred to as the 'side variance', is defined for polygonal cells, with n neighbours and n sides having lengths $\{l_i\}$. The variance $\sigma = \langle l_i^2 \rangle - \langle l_i \rangle^2$ of these n sides is zero when all sides have the same length and increases when the side lengths differ. This quantity has the advantage of keeping track of individual side lengths, a short side which meets two longer sides at each of its ends is likely to side swap. A limitation is that measuring a variance is always more noisy than measuring an average. There is a more serious drawback; consider a hexagon with equal side lengths, some walls concave and some convex in

order to meet at 120° (figure 3(c)). Such a hexagon can be arbitrarily elongated, but σ remains zero. The total variance σ_L of the side length distribution characterizes the whole froth. Equivalently, we can study the average and variance of the difference δl_i of a side's length between two successive images.

The dimensionless perimeter-to-area ratio $P/A^{1/2}$ of each cell measures the wall energy of a cell if its area remains constant. $P/A^{1/2}$ reaches its minimum value $2\pi^{1/2} \approx 3.55$ for a circle and increases as the cell side number decreases, as walls become concave or as the cell elongates. An elliptical cell of given area and small eccentricity $e \ll 1$ has axes a and b such that $b^2 = a^2(1 - e^2)$, a perimeter $P \approx \pi 2a^2(2 - e^2)^{1/2}$ and an area $A \approx \pi a^2(1 - e^2)^{1/2}$, so that the ratio $P/A^{1/2}$ goes as $2\pi^{1/2}(1 + e^4/16) + O(e^6)$.

Other similar analyses do not pertain to our problem. For instance, A/P has the dimension of a length; the correlation between A/P and the cell size is a statistical measurement of a whole foam but does not yield a scale-independent analysis of a single cell's shape. We could have normalized $P/A^{1/2}$ by the $P/A^{1/2}$ value for a regular n -sided polygon $(P/A^{1/2})_n = 2[n \tan(\pi/n)]^{1/2}$, but this normalization is discontinuous when n changes, precisely during the T1 events that we wish to study.

3.2. Actual measurements

In practice, $P/A^{1/2}$ is almost always greater than or equal to the $P/A^{1/2}$ value for a regular hexagon $(P/A^{1/2})_6 = 3.72$. Measuring the deviation of $P/A^{1/2}$ from 3.72 is thus a good compromise between physical meaning and robustness to noise, at low computational cost. We also keep track of the individual side lengths $\{l_i\}$ and describe the topology by the cell side number n . As statistical measures of the whole foam we use σ_L and $\langle P/A^{1/2} \rangle$.

Simulated foams are dry, so that the side length is unambiguous. The residual anisotropy of the underlying weighted next-nearest-neighbour square lattice introduces an error of between 0 and 8% according to the orientation of the wall portion considered with respect to the lattice. The error in perimeter is thus a few per cent. In a foam more polydispersed than ours, with smaller cells and thus larger artefacts due to the pixelization, the ratio $P/A^{1/2}$ could still be robustly determined, because of the Hough transformation (Ballard 1981).

For experimental image analysis, we used software adapted from NIH-Image (Cardoso 1997). The image is first thresholded into black and white pixels to define cell boundaries. A cell perimeter is then measured as the sum of the distance between boundary pixels. For the same image, the measures of perimeter determined with this software, and with the method used in the simulation, differ by a few per cent. The image is then skelitized, by eroding the walls to a thickness of one pixel, and cell sides are defined on the resulting polygonal cells. The size of the vertices is also reduced to one pixel, so that the measure of the side length becomes unambiguous. For an n -sided cell, the measured sum of its n side lengths is highly correlated ($R > 0.99$) with, but n pixels more than, the perimeter measured as above.

§4. RESULTS

4.1. Effect of magnetic field on the elongation of cells

Decreasing the external magnetic field H leads to coarsening. We analysed a series of 21 successive images for the same foam at decreasing H and constant ferrofluid fraction; for instance the series at ferrofluid fraction $\phi = 0.13$ from

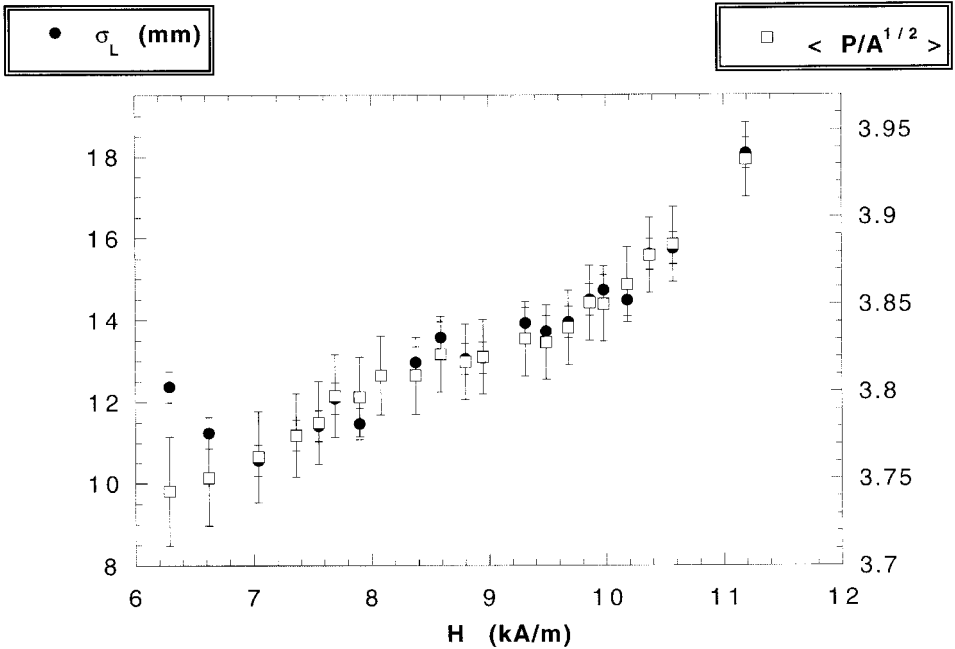


Figure 4. Elongation of cells during froth coarsening, (see figure 2). The variance of cell side length (\bullet), and cell perimeter-to-area ratio (\square) have been averaged over all cells of the foam. Each point is an average over four different foams, made with the same ferrofluid fraction $\phi = 0.13$.

which figure 2 has been extracted. The cell elongation decreases during coarsening. The variance of the cell side length and cell perimeter-to-area ratio correlate (figure 4); the latter is least noisy and conforms better to visual intuition than does the cell side length or cell eccentricity. These three quantities decrease during natural foam evolution. The wall thickness increases, and the foam becomes wetter. As expected, skeletization artificially increases σ_L . In very wet foams, small sides or even fourfold vertices can appear. However, the values of $P/A^{1/2}$ and the results presented in the next section are correct for both dry and wet foams (figure 4). TIs spontaneously occur and reduce the cell elongation.

We also increased H after nucleating the foam. As explained above, the wall lengths increase and cells elongate to increase their perimeter-to-area ratio. Here again, TIs spontaneously occur and reduce the cell elongation.

4.2. Natural and artificial T1 processes

From the same series of pictures of coarsening we extracted successive pictures between which a T1 had occurred, that is each time that one side length reached zero during the natural evolution of the foam. Detailed measurements of wall length before and after a T1 show that the process significantly changes roughly 15–20 walls, depending on the image. Figure 5(b) shows the change in individual wall lengths. Small walls grow and long walls shrink, which confirms that a T1 decreases the average elongation of cells. Simulations display the same behaviour. Both experiments and simulations (figure 6) show that the perturbation of the elongation

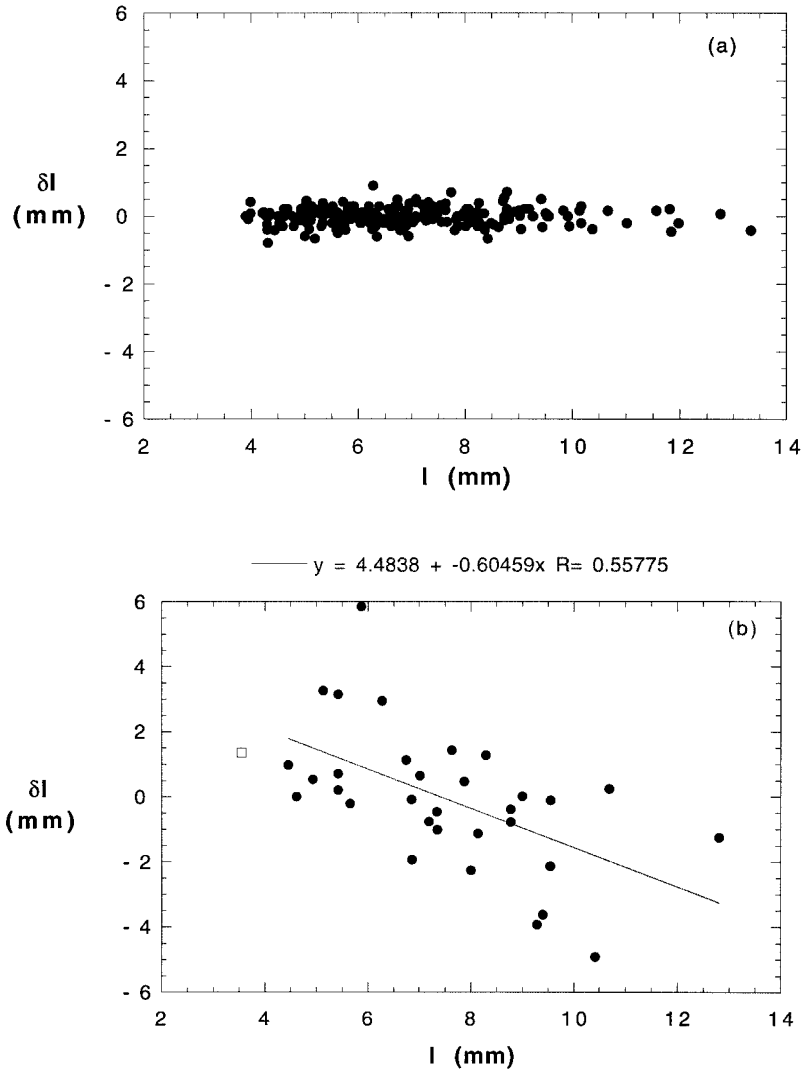


Figure 5. Each dot represents the variation in length of a wall between two images, plotted against the initial length, expressed in millimetres. (a) No side length varies more than 5 mm between two images at fields $H = 9.8 \text{ kA m}^{-1}$ and $H = 9.0 \text{ kA m}^{-1}$ without a T1 between them. (b) 18 side lengths vary significantly between two images at fields $H = 11.2 \text{ kA m}^{-1}$ and $H = 10.6 \text{ kA m}^{-1}$, with one T1 between them; they belong to the 19 cells closest to the T1. Amongst these sides, the shorter sides tend to increase in length while the longer sides tend to shrink, thus reducing the average cell elongation; the straight line is a linear fit through these side changes. (c) Between two images separated by an artificial T1 (see figure 7), 24 side lengths alter significantly, but with no correlation to their original length.

extends over a range of roughly three cell diameters. Nevertheless, the averages of the side length variation over a wall shell surrounding the disappearing wall (figure 6(a)) show that the averaged elongation decreases only in the group of four cells involved in the T1.

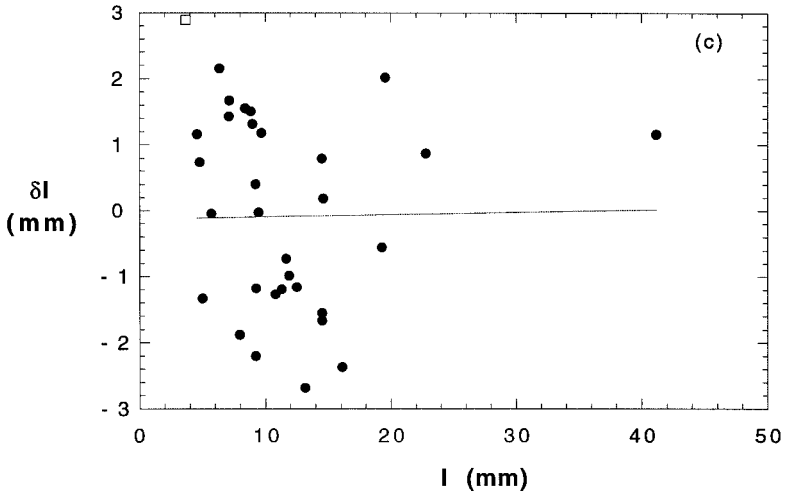


Figure 5.

Given the cell areas, does the selected configuration correspond to the minimum possible energy? Watching a foam does not provide the answer.

Experimentally, we selected a side (figure 7(a)) and placed a metallic pin above it, locally attracting magnetic fluid to create an artificial unstable fourfold vertex (figure 1). After removing the pin, this fourfold vertex spontaneously decayed into one of the two configurations with two threefold vertices. It returned to the initial configuration if it had a lower energy. In a minority of cases, it induced an artificial T1 (figure 7(b)) if the initial, naturally selected configuration had a higher energy than the artificially induced configuration.

These ‘artificial T1s’ did not always decrease the average cell elongation, as in figure 7(a)–(c) and in figure 5(c). The variation in wall length and the initial wall length were uncorrelated. Of course, more elongated cells were much easier to side swap. Comparing the images before and after an artificial T1, we observed that vertices up to the third neighbours around the T1 moved (figure 7(d)); deformation propagated over a finite range.

These motions were due only to the T1. We checked as follows that they were not due to any possible time evolution of the froth. By placing a pin above the newly created side, we made it collapse into a fourfold vertex; then, moving the pin to and fro, we could attract more magnetic fluid and recreate the side which had disappeared (figure 7(c)). After this ‘reverse T1’, all vertices reverted to their original positions and both images were identical (figure 7(e)). The correspondence is probably not a coincidence but rather shows that the initial pattern was nearly equilibrated (a local energy minimum).

4.3. T1 and perimeter-to-area ratio

A detailed analysis of the perimeter-to-area ratio supports and refines the preceding results regarding the decreasing cell elongation induced by a T1.

That a T1 is a short-range process is apparent in (figure 8(c)). In typical images, the two cells which lose a side always have one of the largest $P/A^{1/2}$ values before the T1, and become significantly rounder after the T1 (figure 8(a) and (b)). In fact, the

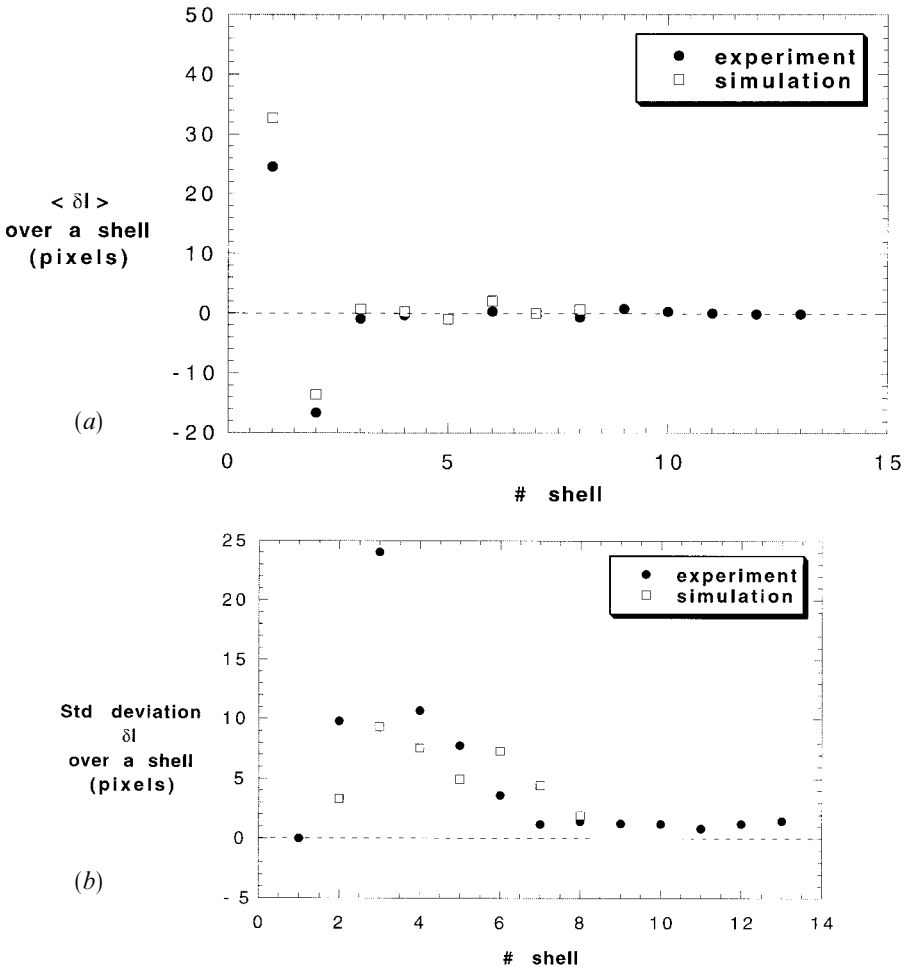


Figure 6. (a) The average side length variation and (b) its standard deviation are measured for each cell wall of a foam before and after a natural T1 process, in an experiment (●) and in a simulation (□). To show the range over which the perturbation due to the T1 extends, the variation for each wall is then averaged over each *wall shell*, defined as follows. Shell 1 is the disappearing or created wall. Walls of shell 2 touch shell 1, walls of shell 3 touch shell 2, and so on. The shells are therefore roughly circular and centred on the disappearing wall. The last affected shell is shell 6 or 7, that is walls which are separated from the T1 by roughly three cell diameters.

sum of the $P/A^{1/2}$ values of the other cells shows no significant variation. Detailed study as a function of cell distance (not shown) confirms that the T1 perturbs $P/A^{1/2}$ over a range of three cell diameters (i.e. up to the sixth shell, as defined in figure 8(c)).

A simulation of a sheared foam is instructive. Starting with a (metastable) equilibrated foam, we apply a steadily increasing bulk shear (Jiang *et al.* 1998). After an initial transient, we see that, on average, $P/A^{1/2}$ increases steadily. The rate and amplitude of the shear are chosen to produce isolated T1s (figure 9(b)), and we can examine the four cells around the T1. During the T1, the cell which has the largest $P/A^{1/2}$ loses one side and its $P/A^{1/2}$ decreases strongly (figure 9(e)). The other cell

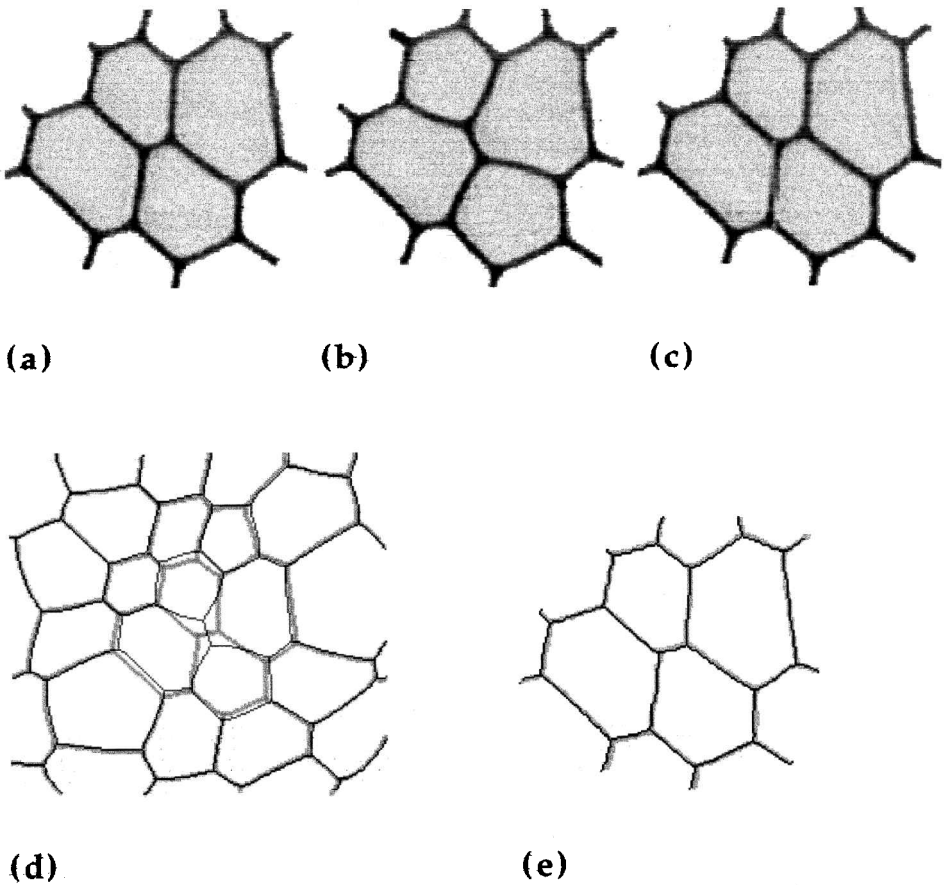


Figure 7. (a), (b) A T1 process is artificially forced in a ferrofluid froth, (see §2.1); (b), (c) then the inverse T1 is forced, to return to the original pattern (c). (d) Superposition of the images (b) after (appears dark) and (a) before (appears grey) the first T1. (e) Superposition of the images (c) after and (a) before both T1s. The images are indistinguishable.

which loses one side also sees its $P/A^{1/2}$ decrease for a few MCSs and then resumes the average growth. The cells which gain one side barely change $P/A^{1/2}$. Averaging over these four cells clearly emphasizes that the T1 transiently reduces the mean value of $P/A^{1/2}$ (figure 9(d)), during a time characteristic of the froth relaxation towards (metastable) equilibrium. The relaxation of the froth after the shear has ceased is similar: when a cell loses one side, its elongation decreases strongly (figure 9(f)).†

The same effects are experimentally observed in a series of four successive T1s (figure 10). The average $P/A^{1/2}$ steadily decreases through each T1, while the $P/A^{1/2}$

† Artificial T1s could also in principle be simulated in a (metastable) equilibrated foam. Running the simulations at a high temperature, the foam explores other states around the local energy minimum. As soon as a fourfold vertex is detected, the foam is quenched by setting the temperature to zero, and the fourfold vertex decays into two threefold vertices.

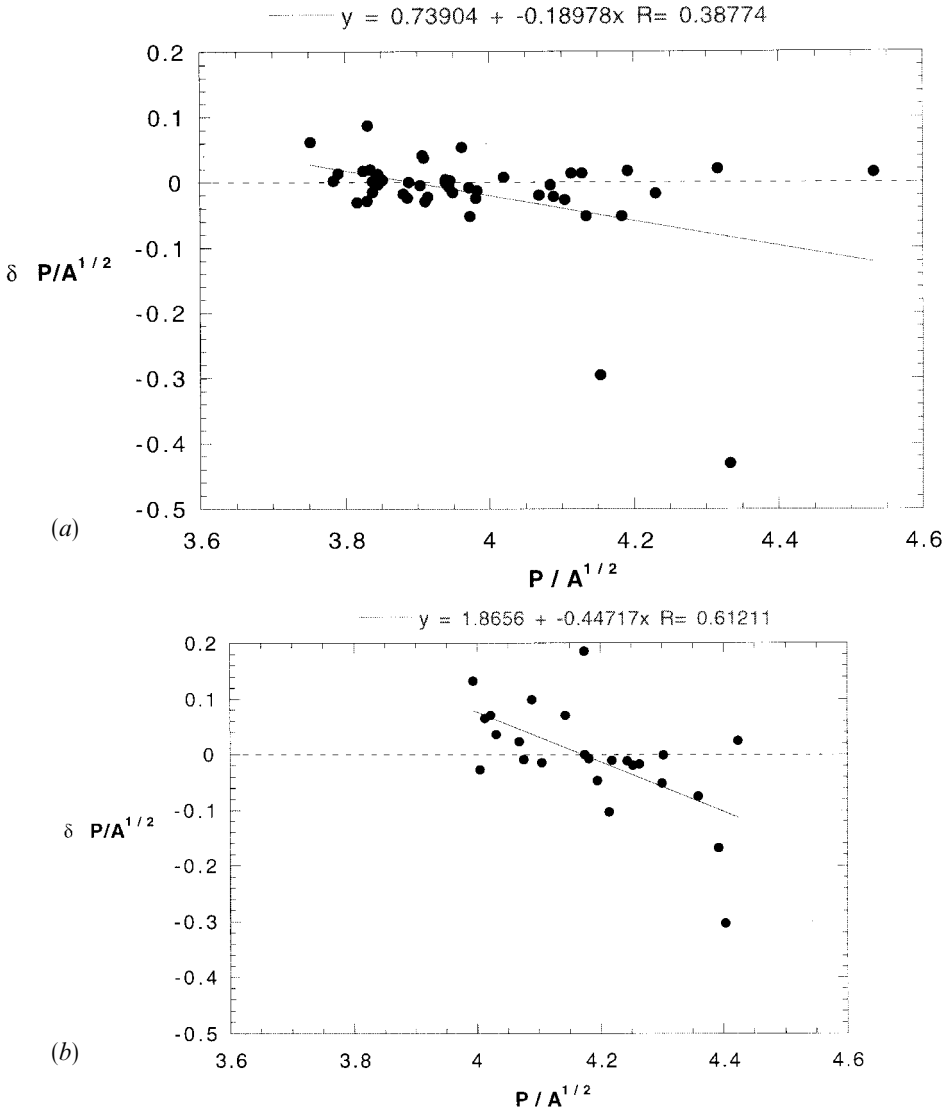


Figure 8. The variation in $P/A^{1/2}$ before and after a natural T1 plotted against its initial value, for each cell, in the same manner as in (figure 5). (a) Experiment ($H = 11.23 \text{ kA m}^{-1}$ before the T1 and $H = 10.98 \text{ kA m}^{-1}$ after). Two cells have a $P/A^{1/2}$ decrease larger than 0.3. (b) Simulation of 26 cells. In this case, the T1 occurs during the relaxation of a non-sheared pattern. (c) The same data plotted as a function of cell distance averaged over *cell shells* (different from the wall shells defined in figure 6), defined as follows: shell 1 contains the two cells which lose one side, shell 2 contains the two cells which gain one side, cells of shell 3 touch shell 1, cells of shell 4 touch shell 2, and so on.

of a cell decreases greatly when a cell loses a side and increases slightly when a cell gains a side. Note that, when a cell loses a side, $P/A^{1/2}$ still decreases over the few next images, implying that the time between successive T1s is comparable with the relaxation time of the froth and that the T1s begin to overlap.

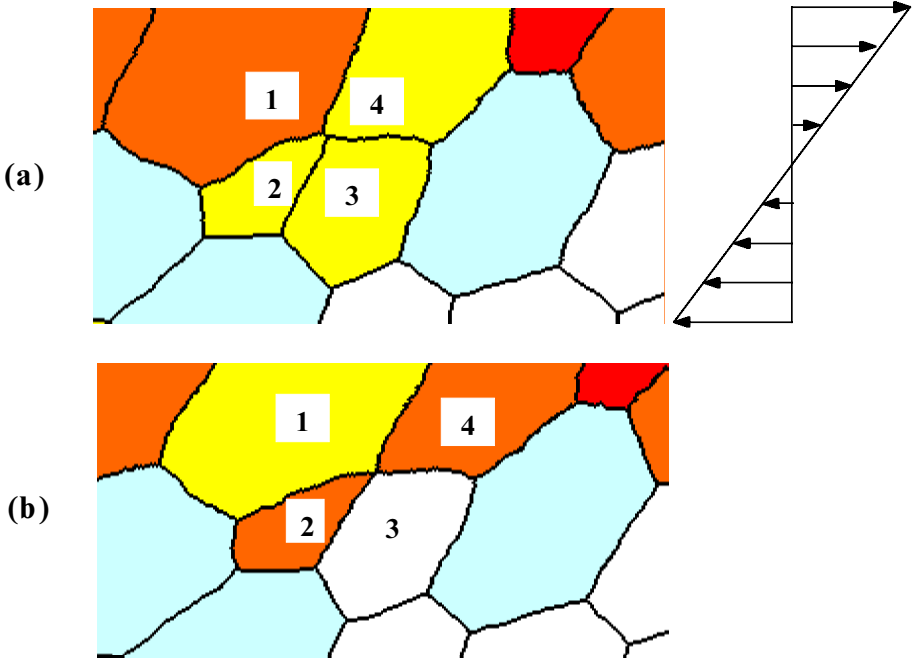
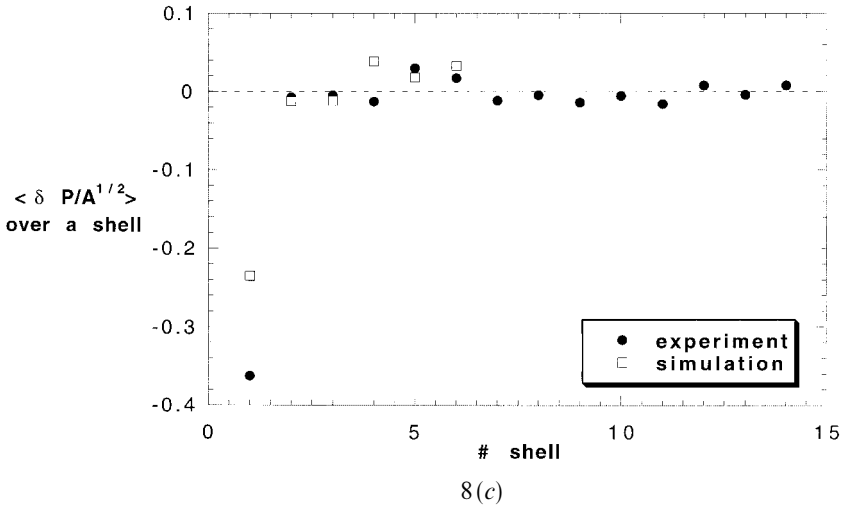
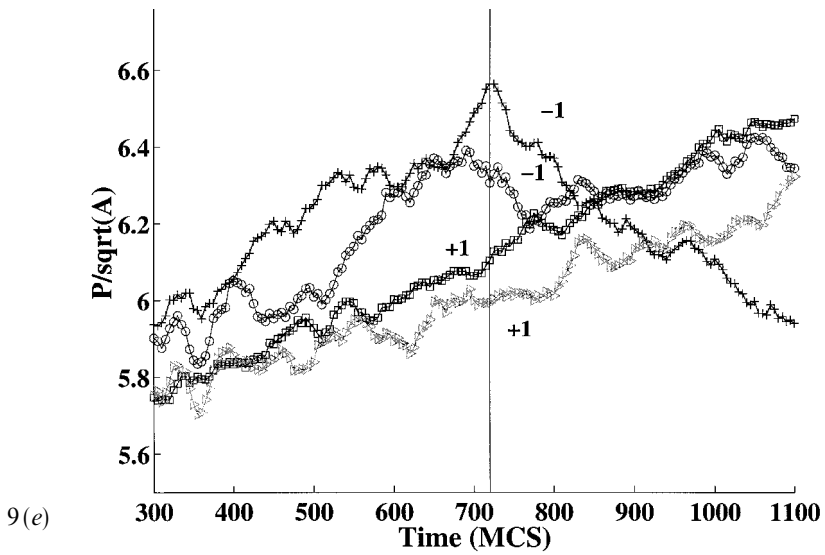
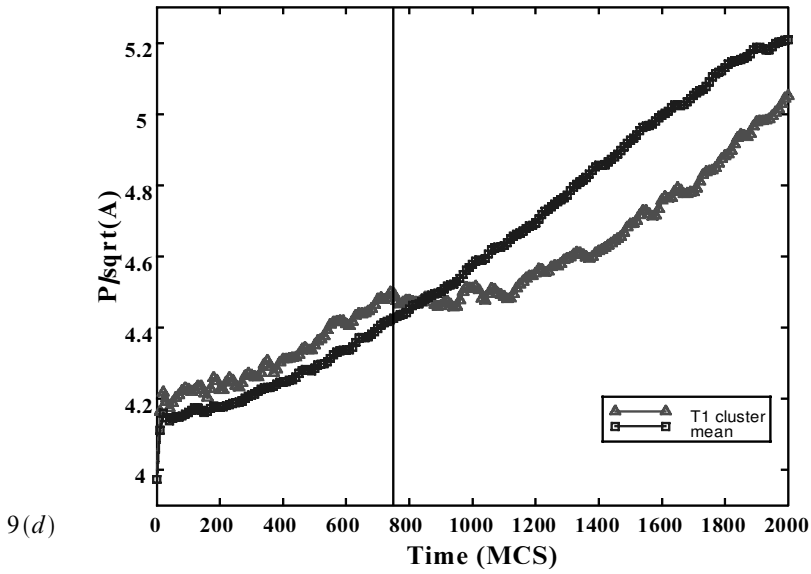
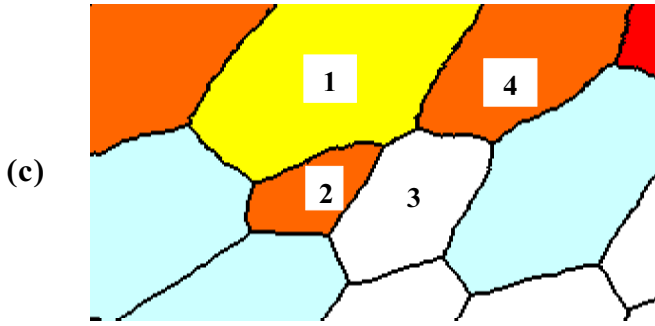
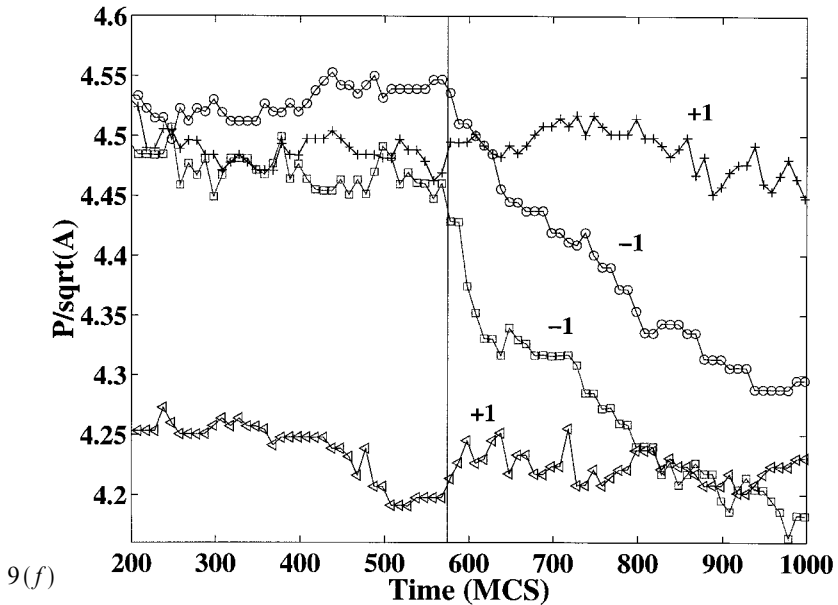


Figure 9. Simulation of a sheared froth: the shear increases the average elongation, until a T1 process relaxes it. (a), (b), (c) Snapshots of a single T1 under bulk shear. The strain rate linearly depends on the vertical position, schematically illustrated beside (a). Grey levels indicate cell side numbers. (a) 550 MCSs, (b) 750 MCSs, (c) 950 MCSs. Cells 1, 2, 3 and 4 elongate under shear. A T1 process (b) reduces the elongation of cells 2 and 4 when they each lose a side. (d) The elongation, $P/A^{1/2}$, averaged over 26 cells (\square) steadily increases under shear. The average elongation over only the four cells involved in the T1 (\triangle) decreases when the T1 occurs (vertical line). (e) Details, cell by cell. Before the T1, the four cell elongations increase under shear like the average. After the T1, the two cells which lose one side ($+$, \circ) decrease $P/A^{1/2}$. The two cells which gain one side (\square , \triangle) do not change $P/A^{1/2}$. (f) Same behaviour during a T1 (vertical line) when the froth relaxes after the shear has been suppressed at $t = 0$ MCS.





§5. MECHANICAL PROPERTIES: AN OPEN PROBLEM

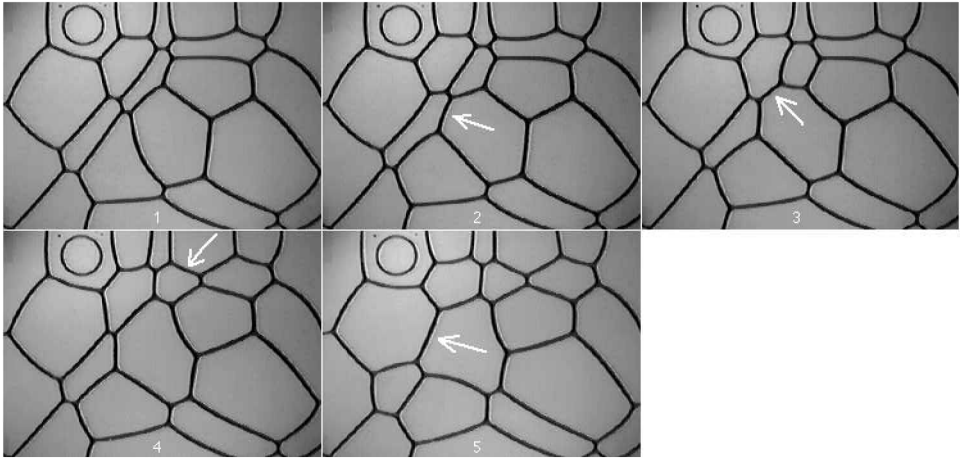
5.1. Probability of a T1

Given a certain perturbation of vertex positions, can we predict where and when T1s will occur? A weaker version of this question is: can we statistically predict the probability of T1 occurrence, that is the number of T1s occurring in a sufficiently large froth? The answer determines the foam's elasticity and time evolution due to diffusion-driven cell area changes; it should depend on the topological and geometrical disorder of the foam, that is the variances of cell topology and side length. We now discuss the effect of a vertex displacement over a distance Δ , either smaller or larger than a typical cell side length.

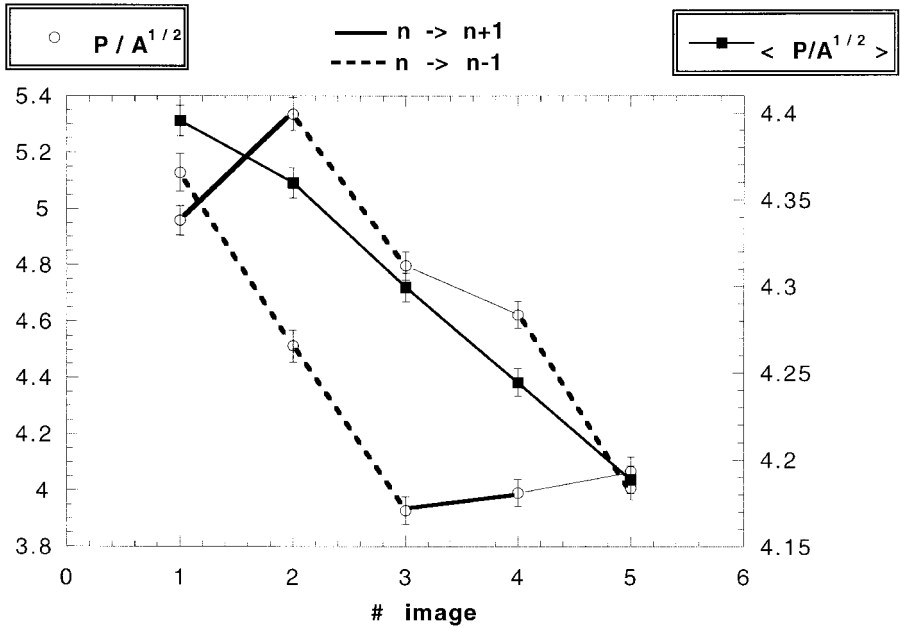
5.2. Effect of a small vertex displacement

By displacing a vertex over a distance Δ smaller than the typical cell size, we can determine the response function of the foam. We characterize it by measuring the displacement $\delta(\Delta, r)$ of another vertex, at a distance r from the perturbation. $\delta(\Delta, r)$ depends only on the intrinsic properties of the foam at the time considered.

In experiments (figure 11) and simulations (M. Asipauskas, private communication), an artificial vertex displacement over a small Δ induced displacements of the neighbouring vertices over a range of three typical cell diameters, the same range as for T1s (§4.2). The response function of the foam is elastic and linear, for each vertex, δ is proportional to Δ (figure 11). However, δ is not a simple power law in r and is not even a single-valued function of r . Moreover, the induced displacements have widely distributed orientations and strongly depend on quantities which vary simultaneously: the relative orientations of the walls and the displacement Δ , and the cell areas and pressures.



(a)



(b)

Figure 10. (a) A foam where elongated cells have been artificially nucleated and then spontaneously relaxed through four T1 processes causally related in a chain reaction. Since the typical time scale of a T1 is about 1s, well separated images were captured between each T1; the white arrows indicates each new side. (b) The plots show $P/A^{1/2}$ for two individual cells, indicating where they gained (+1) or lost (-1) a side, as well as the average $\langle P/A^{1/2} \rangle$ over the whole foam (■).

5.3. Effect of a large vertex displacement

A T1 results in an effective vertex displacement Δ of two vertices. Δ can be defined as half the size of the newly created side and is comparable with an average side length. What is the response function $\delta(\Delta, r)$ of the foam to this finite value of Δ ?

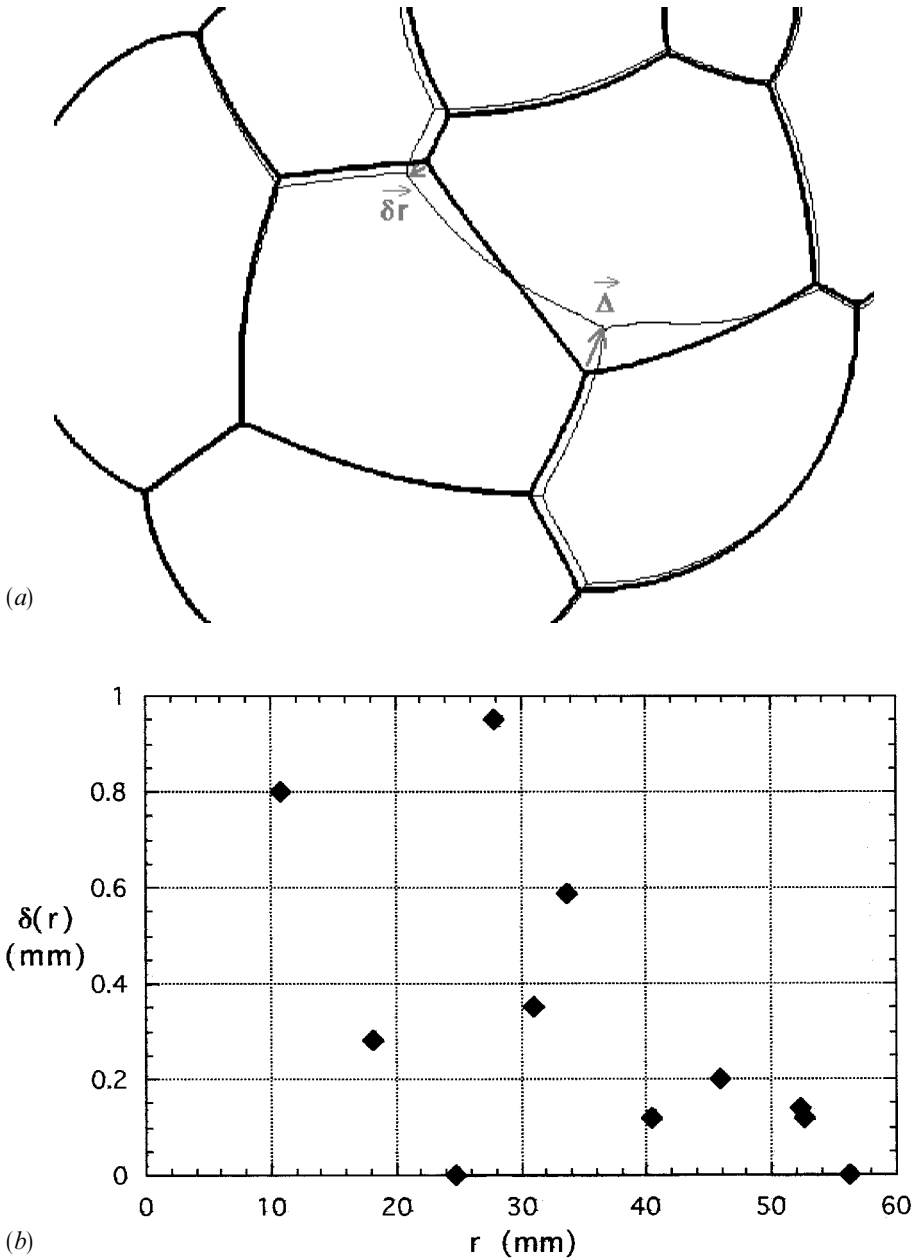
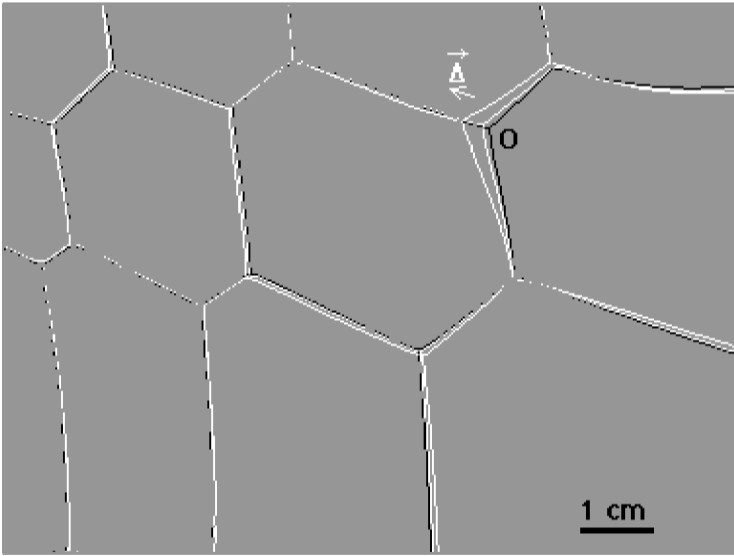


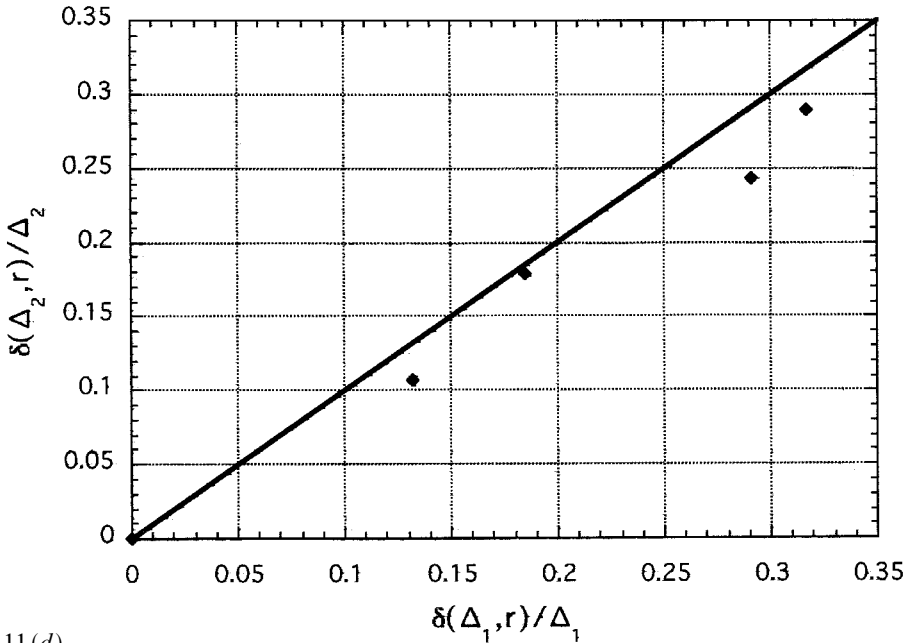
Figure 11. (a) Skeletized images of a ferrofluid froth in (metastable) equilibrium (thick lines) and after an additional external magnetic force has displaced the vertex O over a distance Δ (thin lines). (b) The displacement $\delta(\Delta, r)$ of a vertex is not simply a function of the distance r to the perturbation. (c) Image of another ferrofluid froth in (metastable) equilibrium (black lines). A vertex has been displaced over two different values of Δ in the same direction (white lines); $\delta(\Delta, r)$ appears roughly proportional to Δ . (d) Points lie close to the first diagonal (one symbol = one vertex, values of $\delta < 0.07$ mm are not shown). (e) Similar diagram for another experiment. A vertex has been displaced over three different values of Δ in the same direction. Perturbation $\Delta_1 = 2.3$ mm upwards; perturbation $\Delta_2 = 5.9$ mm downwards (\blacklozenge); perturbation $\Delta_3 = 5.15$ mm downwards (\diamond).



11(c)

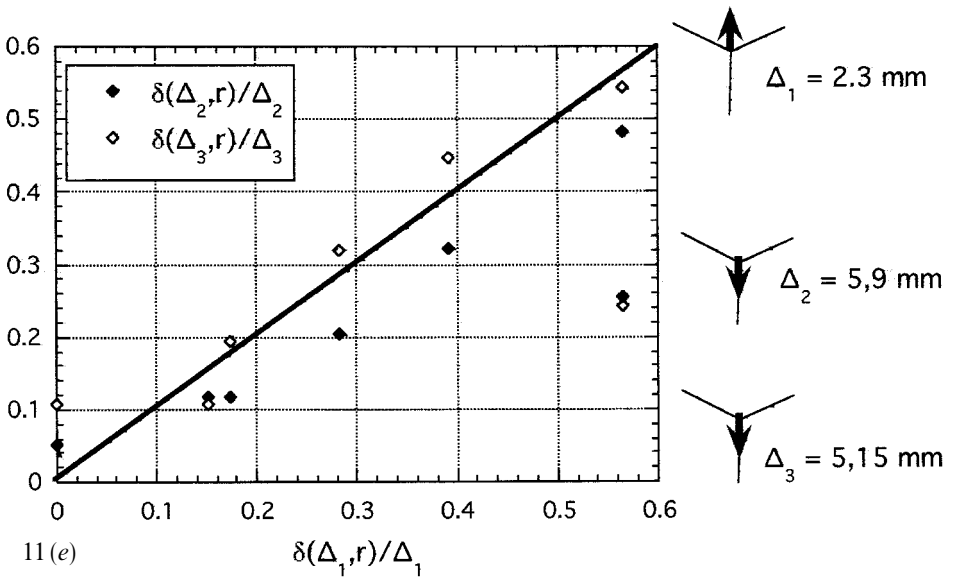
$$\Delta_1 = 0.89 \text{ mm}$$

$$\Delta_2 = 3.29 \text{ mm}$$



11(d)

As in §5.2, a T1 does *not* induce a quadrupolar displacement field, which would be expected in a homogeneous isotropic medium. Since a small displacement of a vertex can trigger a T1, which in turn can create a large displacement of neighbouring vertices, the question is now: under what conditions does an initial vertex displacement trigger an avalanche of T1s?



A hand-waving argument hints at an answer, which depends on the topological and geometrical disorder of the foam and remains to be quantitatively studied:

- (1) Consider first a perfect regular hexagonal lattice, with all sides of length L . Only when a vertex is moved over $\Delta \geq L$ can it trigger a T1. In turn, it will create a displacement of order L , its neighbours will be even less displaced and there will be no avalanche. In that sense, the regular lattice is not 'excitable'.
- (2) The same holds for a foam with almost uniform cell areas, close to this hexagonal configuration, that is monodispersed in side lengths and side numbers. Only a few cells lie within the range of the perturbation induced by a T1, only a small proportion of which can undergo another T1.
- (3) A foam with a very broad area distribution satisfies the condition for triggering an avalanche; within a small enough distance r from the T1, lie sufficient sides of small enough length L that $\delta(\Delta, r) > L$. If one of the largest cells side swaps, an avalanche might affect many neighbouring small cells. Such an avalanche remains confined to a small fraction of the entire foam. Its effect on the foam's mechanical properties is weak.
- (4) Only a foam with a monodispersed distribution of cell areas but a very dispersed distribution of cell side lengths constitutes a more interesting 'excitable medium' (figure 10). Here an avalanche can propagate over the whole foam, until all cells are rounder and have a low $P/A^{1/2}$, significantly affecting its mechanical properties.

§6. CONCLUSION AND DISCUSSION

Taking advantage of ferrofluid foams, in which side-swapping (T1) processes are very easy to isolate, observe, force and reverse, we have obtained the following results.

- (1) For given cell areas, a foam relaxes towards an equilibrated pattern, and its surface energy reaches a local minimum. This energy minimization is deterministic.

- (2) The energy minimum is not always the global minimum (lowest energy) compatible with the cell areas. The naturally selected pattern is metastable, but not necessarily stable.
- (3) Estimating the difference between the foam energy and its global minimum value is difficult. In ferrofluid foams and simulations, the total wall length variation during relaxation is less than 1%, even when a T1 occurs, and it is thus sensitive to pixelization. Only during the relaxation of an (artificial) foam very far from its global energy minimum, such as in (figure 10), could we measure a significant variation in the total wall length. Moreover, the global minimum value itself is usually not known.
- (4) On the other hand, in a metastable pattern, the cell elongation correlates with the deviation from the global energy minimum. The dimensionless perimeter-to-area ratio $P/A^{1/2}$ is easily measured for a single image, without prior knowledge of the foam's past or future evolution. It is a good measure of cell elongation. Its minimum value is known; the theoretical lower bound is 3.55 and in practice it seldom falls below 3.72. As such, it is a convenient tool for visualizing stress fields.
- (5) Natural T1s, which correlate with the geometry and not the topology of the foam, decrease cell elongation. The cell which has the highest $P/A^{1/2}$ is likely to lose a side and decrease its $P/A^{1/2}$, while cells which gain sides will slightly increase their $P/A^{1/2}$ values. This result is not an artefact due to the variation with n in the $P/A^{1/2}$ value for a regular n -sided polygon: $(P/A^{1/2})_n = 2[n \tan(\pi/n)]^{1/2}$. In fact, since $(P/A^{1/2})_n$ decreases with increasing n , the normalized value $(P/A^{1/2})/(P/A^{1/2})_n$ shows an even larger variation than $P/A^{1/2}$ does. It would be instructive to investigate the correlations between the elongations of the side-swapping cells and of their neighbours.
- (6) That artificial T1s do not decrease cell elongation suggests a causal relation between elongation and natural T1s.
- (7) Natural T1s, artificial T1s and reverse T1s induce non-local but short-range perturbations.
- (8) T1s affect the geometry, not only of the cells which side swap, but also of about a dozen of their neighbours. $P/A^{1/2}$, the side length variance σ and vertex displacements vary for cells within three typical cell diameters of the T1.
- (9) When displacing a vertex over a small distance Δ , the displacement $\delta(\Delta, r)$ of another vertex, at a distance r from the perturbation, is linear in Δ and reversible. Predictions of $\delta(\Delta, r)$ could rely on the analytical minimization of energy for the positions of two vertices while all their neighbours are kept fixed. Since experiments prove that the perturbation has a finite range, an iteration by letting every possible vertex pair move should eventually converge. Simulations could help to identify the role of disorder and boundary conditions.

Understanding the spontaneous decrease of 2D cell elongation through T1s might determine whether, starting from an arbitrary initial froth, the distribution of cells' elongation relaxes until it reaches a (possibly universal) predictable distribution. By generalizing the definition of elongation as surface/(volume)^{2/3}, this study might be extended to 3D cells.

Note added: Since we submitted this paper, a paper by Szeto *et al.* (1998) has recently been published. It shows that non-zero correlations exist between cells up to the third shell at least. This agrees with our findings.

ACKNOWLEDGEMENTS

We would like to thank Sophie Neveu for providing us with the magnetic fluid, Marius Asipauskas for his participation in simulations, Jean-Claude Bacri for his friendly support, Olivier Cardoso for the image analysis, and Norbert Kern for critical reading of the manuscript. J. A. G and Y. J. acknowledge support from the American Chemical Society/Petroleum Research Fund and National Science Foundation/National Young Investigator Award DMR-92-57011.

REFERENCES

- BALLARD D., 1981, *Pattern Recognition*, **12**, 2.
 CARDOSO, O., 1997, NIH-Image.†
 ELIAS, F., DRIKIS, I., CEBERS, A., FLAMENT, C., and BACRI, J.-C., 1998a, *Eur. Phys. J. B*, **3**, 203.
 ELIAS, F., FLAMENT, C., BACRI, J.-C., CARDOSO, O., and GRANER, F., 1997, *Phys. Rev. E*, **56**, 3310.
 ELIAS, F., FLAMENT, C., BACRI, J.-C., and GRANER, F., 1998b, in *Foams and Emulsions*, edited by J. F. Sadoc and N. Rivier (Deventer: Kluwer).
 GLAZIER, J. A., 1989a, PhD Thesis, The University of Chicago; *Phys. Rev. Lett.*, **70**, 2170.
 GLAZIER, J. A., ANDERSON, M. P., and GREST, G. S., 1990, *Phil. Mag. B*, **62**, 615.
 HOLM, E., GLAZIER, J. A., SROLOVITZ, D. J., and GREST, G. S., 1991, *Phys. Rev. A*, **43**, 2262.
 JIANG, Y., SWART, P. J., SAXENA, A., ASIPAUSKAS, M., and GLAZIER, J. A., 1998, (submitted).
 KRAYNIK, A. M., 1988, *Ann. Rev. Fluid Mech.*, **20**, 325.
 SZETO, K., ASTE, T., and TAM W., 1998, *Phys. Rev. E*, **58**, 2656.

† A user module has been added to this freeware for the analysis of cellular patterns, and is available at <http://www.lps.ens.fr/~cardoso/>. NIH-Image is freeware. O. Cardoso (Laboratoire de Physique Statistique Ecole 752e Normale Supérieure de Paris) modified this freeware in 1997 and put it on the web.